Cross-reacting material 197 (CRM197) affects actin cytoskeleton of endothelial cells

Bilge Özerman Edis[1], Başak Varol[1], Ebru Haciosmanoğlu[1,2], Ayhan Ünlü[1,3] and Muhammet Bektaş[1]

[1] *Department of Biophysics, Istanbul Faculty of Medicine, Istanbul University, 34390 Çapa, Istanbul, Turkey*
[2] *Department of Physiology, Faculty of Medicine, Istanbul Bilim University, 34394 Esentepe, Istanbul, Turkey*
[3] *Department of Biophysics, Faculty of Medicine, Trakya University, 22030 Edirne, Turkey*

Abstract. CRM197, cross-reacting material 197, is a mutant of diphtheria toxin (DTx). CRM197 is used in pharmacology as a carrier protein. It has been recently shown that CRM197 causes breakdown in actin filaments. In order to show intracellular localization of CRM197 and visualize cell structure via actin cytoskeleton, endothelial cells were cultured and subjected to CRM197 *in vitro*. To address the interaction between CRM197 and actin both experimental and theoretical studies were carried out. Colocalization of CRM197 with actin filaments was determined by immunofluorescence microscopy. Following 24-hour incubation, the loss of cell-cell contact between cells was prominent. CRM197 was shown to bind to G-actin by gel filtration chromatography, and this binding was confirmed by Western blot analysis of eluted samples obtained following chromatography. Based on crystal structure, docked model of CRM197-actin complex was generated. Molecular dynamics simulation revealed that Lys42, Cys218, Cys233 of CRM197 interacts with Gly197, Arg62 and Ser60 of G-actin, respectively. CRM197 binding to G-actin, colocalization of CRM197 with actin filament, and actin cytoskeleton rearrangement resulting in the loss of cell-cell contact show that actin comes into sight as target molecule for CRM197.

Key words: Actin filaments — Cross-reacting material 197 — Diphtheria toxin — Endothelial cells

Abbreviations: CRM197, cross-reacting material 197; DTx, diphtheria toxin; FA, fragment A; HUVEC, human umbilical vein endothelial cells.

Introduction

CRM197 is mutant of diphtheria toxin (DTx), a family member of binary toxins. CRM197 (58.4 kDa) contains two subunits like DTx. CRM197 lacks the enzymatic activity due to a single amino acid substitution (Gly52 to Glu) in fragment A (FA), and this substitution yields a non-toxic product (Giannini et al. 1984). In cytosol, fragment A, the catalytic domain of native toxin, transfers ADP-ribose moiety of NAD to eEF2 and causes the halt of protein synthesis whereas the mutation in CRM197 prevents enzymatic activity, thus protein synthesis continues (Kageyama et al. 2007). CRM197 has been effectively used in vaccines as a carrier protein or as an immunological adjuvant (Shine-

field 2010). CRM197 maintains its binding ability to DTx receptor which is a transmembrane protein, EGF receptor heparin-binding epidermal growth factor-like growth factor (HB-EGF). CRM197 can bind to either membrane anchored (proHB-EGF) or soluble forms (S-HB-EGF). proHB-EGF takes role in cell-cell adhesion, and secreted HB-EGF has mutagenic activities (Vinante and Rigo 2013). HB-EGF gene expression is up-regulated in oncogenic transformations, and anti-tumor properties of CRM197 binding to HB-EGF have been described in details (Bröker et al. 2011). The cytotoxic effect of CRM197 expression has been also showed in Chinese hamster ovary cells and mouse fibroblast cell line LMTK (Qiao et al. 2008). CRM197 emerges as a chemosensitizing agent for paclitaxel-resistant ovarian carcinoma cells (Tang et al. 2016). The ability of cargo transfer of CRM197 across blood brain barrier provides new opportunities in drug delivery development for central nervous system diseases (Chen and Liu 2012). Intracellular trajectory of native toxin has been studied in details but FA of CRM197 has not

Correspondence to: Bilge Özerman Edis, Department of Biophysics, Istanbul Faculty of Medicine, Istanbul University, 34390 Çapa, Istanbul, Turkey
E-mail: bilge.edis@istanbul.edu.tr

been illustrated so far. Receptor-mediated endocytosis of DTx is followed by FA translocation across the endosomal membrane which is supported by cellular proteins including actin filaments and eukaryotic elongation factor 2 (eEF2) (Varol et al. 2013). FA was determined to interact with both filamentous actin (F-actin) and globular actin (G-actin) in stoichiometric manner (Bektaş et al. 2009; Varol et al. 2012). The most possible interaction has been anticipated by molecular dynamics simulations between Tyr204 of native toxin and Gly48 of G-actin (Ünlü et al. 2013). The binding of FA to F-actin has been proposed to situate at the positive end of the filament (Bektaş et al. 2009). Consequently, FA-actin binding inhibits polymerization which induces the collapse of filament in time. The damaging effect of CRM197 on F-actin has been also reported. Cell lysates of 18 hour CRM197-treated cells have been subjected to the fragmentation of actin and a decrease of 65% in the amount of F-actin has been determined in post-microsomal pellets. Moreover F-actin and G-actin levels have been estimated from the triton-soluble filamentous actin and an increase of 50% in fragmentation of actin has been reported (Varol et al. 2012). In this study, we aimed to show intracellular distribution of CRM197 and cytoskeleton changes in cultured human umbilical vein endothelial cells (HUVEC). We are also showing protein-protein interaction between CRM197 and actin by means of gel filtration analysis and computational techniques for prediction.

Materials and Methods

Materials

All reagents were purchased from Sigma (St. Louis, MO, USA). The murine monoclonal antibody 7F2 reacting with DTx fragment A subunit (anti-FA) was purchased from Abcam (Cambridge, UK) and actin-specific monoclonal antibody (mouse) from Santa Cruz Biotech (Santa Cruz, CA, USA). Sodium boro[^{3}H]hydride, specific activity 15 Ci/mM, was obtained from Perkin Elmer (Waltham, MA, USA). G-actin was prepared as previously described (Bektaş 2009).

Immunofluorescence microscopy and imaging

HUVEC (ATCC-CRL-1730) were grown to semi-confluence on poly-L-lysine-coated coverslips in 6-well plates. Following 24 hour incubation, CRM197 (0.8 nM) was added to the wells. Medium was discarded after 15 minutes of mutant toxin treatment, and cells were washed with phosphate-buffered saline (PBS). Cells were permeabilized in 0.01% Triton X-100 in PBS for 5 minutes at room temperature, and were fixed in 2% paraformaldehyde in PBS for 30 minutes at 4°C. Cells were washed with PBS again, and incubated

with blocking buffer (1% BSA in PBS) for 1 hour. In order to detect CRM197, cells were incubated with the murine monoclonal antibody 7F2 specific to FA. After washed with PBS cells were incubated with fluorescein isothiocyanate (FITC)-labeled goat anti-mouse Ig antibody. Next, F-actin was detected by using phalloidin-TRITC. F-actin staining was carried out also for 24 hour incubation of CRM197 (0.8 nM). HUVEC were mounted on glass with anti-fade reagent with DAPI, and were analyzed on Olympus BX51 Research Microscope with 100× oil-immersion lens. Images were obtained with a DP72 camera controlled by Olympus DP2-TWAIN software.

Analysis of cell-cell contact areas

To analyze cell-cell contact areas, the area between endothelial cells ($n = 10$) was measured by Olympus DP2-TWAIN software. Data from diverse locations ($n = 27$) were presented as means ± SD. The unpaired t test was used to compare differences between control and CRM197-treated cells. Statistical significance was accepted for $p < 0.05$.

Reductive tritiation of CRM197

CRM197 (100 mg) was incubated in the presence of 3 mM sodium boro[^{3}H]hydride for 1 hour at 20°C in 50 mM Tris-HCl, pH 7.4. Following incubation, the sample was dialyzed and 10 ml aliquot applied to GF/A filter (Whatman). Glass fibre filters that were washed successively in cold 5% TCA, ether-ethanol (v/v: 1/1) and ether. After drying, the filters were transferred to vials containing 5 ml of 0.4% 2,5-diphenyloxazole in toluene and TCA-precipitated radioactivity was determined in a liquid scintillation counter (Packard Tri-Carb1000 TR). The specific activity of [^{3}H]CRM197 was specified as 8860 dpm/μg. [^{3}H]CRM197 (30 μg) was incubated with G-actin (20 μg) for 1 hour at room temperature in homogenization buffer (5 mM potassium phosphate, pH 7.5, 0.5 mM ATP, 0.1 mM CaCl$_2$, 0.5 mM dithiothreitol and 1 mM NaN$_3$) and then subjected to gel filtration.

Gel filtration analysis

Size distributions were analyzed on a Sephacryl S-100 (Hi-prep 16/60) (GE Healthcare) column equilibrated on an AKTA Prime Plus System with homogenization buffer and calibrated using ribonuclease (Mr 13.7 kDa), carbonic anhydrase (Mr 29 kDa), ovalbumin (Mr 43 kDa), conalbumin (Mr 75 kDa), phosphorylase b (Mr 97 kDa) and β-galactosidase (Mr 116 kDa). The chromatography was monitored using PrimeView software (GE Healthcare Bio-Sciences). Equilibrated column had run at 0.8 ml/min with homogenization buffer and the fraction volume was 1 ml. Tritiated CRM197 was subjected first to gel filtration then

followed by [3H]CRM197-binding to actin. The radioactivity in aliquots from the fractions was determined in 1 ml Bray's solution in a liquid scintillation counter. Column fraction number 43 corresponding to 101 kDa was concentrated using IVSS vivaspin 2 (Sartorius Stedim Biotech, Aubagne, France), centrifugal concentrator, next analyzed by electrophoresis and Western blotting.

Electrophoretic analysis and Western blotting

Sodium dodecyl sulfate-polyacrylamide gel electrophoresis (SDS–PAGE) was performed as described in Laemmli (1970) and followed by Western blotting to detect actin and fragment A of CRM197. PageRuler Prestained Protein Ladder from Thermo Scientific was used as molecular weight standards. Proteins were stained with Coomassie brillant blue and destained in 10% acetic acid, 50% methanol. SDS–PAGE separated proteins were transferred to nitrocellulose (Millipore, MA, USA) membranes which had been prior blocked with TBS (Tris-buffered saline) Tween (TBST) and 0.5% BSA (bovine serum albumin) for 1 hour. The membranes were incubated with actin-specific antibody or FA-specific monoclonal antibody 7F2 and then with alkaline phosphatase conjugates of anti-mouse IgG antibody. After three washes with TBST protein bands on nitrocellulose membranes were detected by NBT/BCIP (nitro blue tetrazolium/5-bromo-4-chloro-3-indolyl phosphate).

Computational determination for CRM197-actin interaction

High-resolution crystal structures and primary sequences of CRM197 and actin were found in Protein Data Bank (PDB). PDB code: 4EA0 for CRM197 (Malito et al. 2012) and 3HBT for G-actin (Ünlü 2014) were used for protein-protein docking. Pymol and VMD with NAMD (academic version of protein analysis software) were used in order to display possible interaction surfaces of CRM197-actin complex by mapping related residues of proteins. For molecular docking protein-protein module PIPER (Kozakov et al. 2006) and ClusPro 2.0 (Comeau et al. 2004) were used as docking algorithms which are available on protein-protein docking system at Structural Bioinformatics Laboratories of Boston University. PIPER uses Fast Fourier Transform (FFT) correlation approach which provides precise pairwise potentials thus the number of false positive poses are critically reduced. The scoring function applied in PIPER is assumed as the totality of terms indicating shape complementarity, desolvation and electrostatic contributions. On the other hand ClusPro 2.0 orders the poses given to their clustering properties. Interaction areas were explored firstly by using a simplified energy model and the theory of restricted flexibility. Then detailed scoring and sampling allowed focusing on determined areas. Next step of algorithm works for validating the docking algorithm by using RMSD (root mean square deviation) and double logic RMSD was used to measure the quality of clustering of structures where clustering means isolation of energy basins of highly loaded energy areas. Docking calculations were completed in PIPER, DARS (Decoys as the Reference State) and SDU (Semi-Definite programming based Underestimation) respectively. In order to find possible conformations, DARS is used to produce reference conditions and free energy stability was analyzed by SDU which provides energy optimization and removing of nonlocal clusters. ClusPro filters the docked confirmations with near-native structures and ranks them based on their clustering properties. The server outputs the top 10–30 docked complexes with highest ranks. By evaluating ten interaction areas according to thermo dynamical energy calculations, areas where the possibility of bonding is high are determined. To analyze ClusPRO theoretical results, docking system was used. These analyzes between CRM197-actin complex structures was done using Z-dock. The Z-dock is a rigid body based docking protocol, which uses a FFT algorithm to perform a 3D searching all possible binding modes in the translational and rotational space between the two protein structures (Pierce et al. 2011).

The free intermolecular binding energy between CRM197 and actin was calculated using NAMD. A total of 1000 frames which were generated at the end of the molecular dynamic simulation were used for the calculation. The free energy of binding between the complexes DG$_{binding}$ was calculated in CHARMM:

$$\Delta G_{binding} = \Delta G_{complex} - (\Delta G_{receptor} + \Delta G_{ligand})$$

In order to study the structural consequences, MD simulations and resulting trajectory files were analyzed for RMSDs.

Results

Breakdown of actin cytoskeleton under CRM197 treatment

CRM197 distribution in endothelial cells was detected by means of FA (Fig. 1A, C). Immunostaining of FA revealed that CRM197 was dispersed all over the HUVEC and F-actin staining showed the colocalization of CRM197 with actin cytoskeleton in 15 minutes of incubation (Fig. 1B, C). Following 24-hour incubation with CRM197 (0.8 nM), F-actin staining was revealed the loss of cell-cell contact (Fig. 1E). Cell-cell contact areas were analyzed and the area between endothelial cells ($n = 10$) was measured by Olympus DP2-TWAIN software. Data from diverse locations ($n = 27$) were presented as mean ± SD. The unpaired t test was used to compare differences between control and CRM197-treated
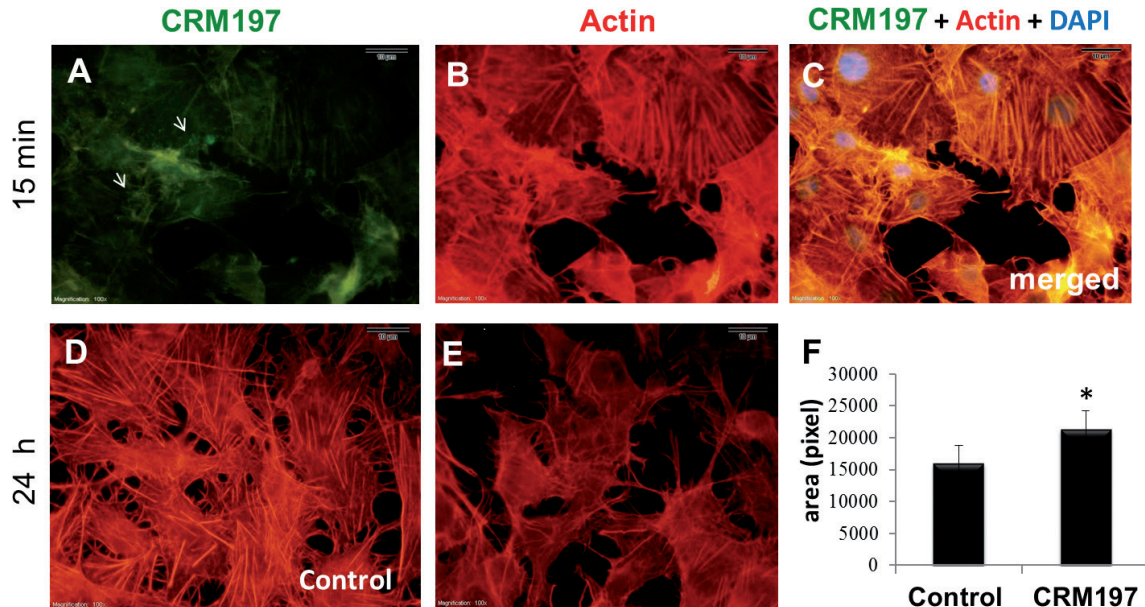
Figure 1. CRM197 treatment in HUVECs. CRM197 (green; **A, C**), F-actin (red; **B, C, D, E**) and nucleus (blue; C). Arrows indicate widespread distribution of CRM197 (A) following 15 minutes of incubation. D and E show F-actin staining in HUVECs incubated 24 hours in the absence (control; D) and in the presence of CRM197 (0.8 nM; E). **F.** Loss of cell-cell contact through areas between cells measured by Olympus DP2-TWAIN software.* $p < 0.05$ *vs.* control, t test.

cells. Statistical significance was accepted for $p < 0.05$. F-actin staining for HUVEC in the absence (control; Fig. 1D) and in the presence of CRM197 (Fig. 1E) for 24 hours of incubation exposed considerable changes in cell-cell contact areas (Fig. 1F). Changes in cell shape due to actin cytoskeletal organization were established significant.

Interaction of CRM197 with actin in vitro

CRM197 was shown to bind to G-actin by gel filtration on Sephacryl S-100. Upon incubation of tritiated CRM197 and G-actin, [3H]CRM197-actin complex became apparent as a new peak (Fig. 2A; dashed line) eluting in a region cor-
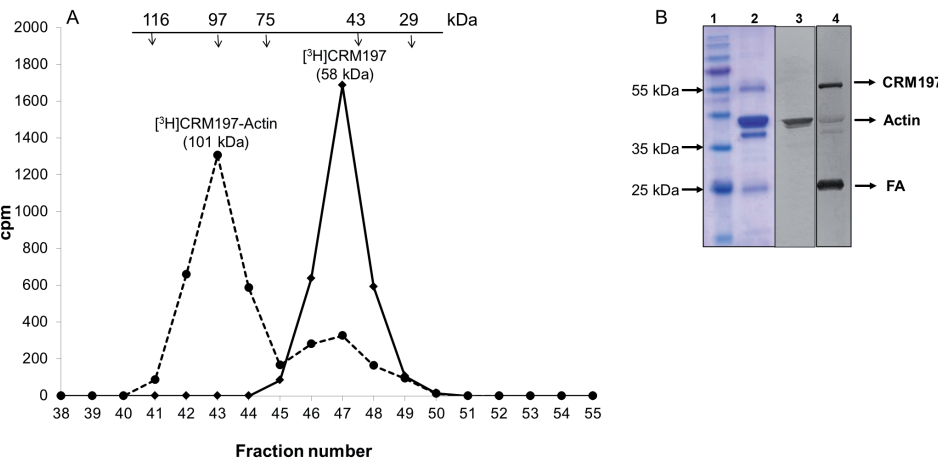

Figure 2. Binding of CRM197 to G-actin. **A.** Superposition of the size exclusion chromatograms of [3H]CRM197 (solid line) and [3H]CRM197-actin complex (dashed line). Arrows indicate the peaks of eluted protein markers (in kDa) of known molecular mass. [3H]CRM197-actin complex became apparent in a region corresponding to about 101 kDa (1st peak) and free [3H]CRM197 (shoulder of 1st peak) stayed at the same region as [3H]CRM197 alone (peak of solid line). Radioactivity (count per minute, cpm) was determined in a liquid scintillation counter. **B.** SDS-PAGE showed proteins profile of gel filtration analysis. Lane 1: prestained molecular mass standards, lane 2: Coomassie dye-staining of proteins eluted from concentrated fraction number 43. The sample on lane 2 was subjected to Western blot analysis using anti-actin (lane 3) and anti-FA (lane 4).

responding to about 101 kDa with a concomitant decrease in sizes of peaks corresponding to [^{3}H]CRM197 (Fig. 2A; solid line). A shift of nearly 70% radioactivity from 58 kDa to 101 kDa molecular weight region was determined. Electrophoretic analysis and Western blotting indicated the presence of actin and CRM197 in the sample eluted from gel filtration (Fig. 2B). Concentrated fraction number 43 was subjected to SDS-PAGE (10 μg *per* well) and Western blotting. Following a reduction of internal disulfide bond during electrophoresis, protein profile of CRM197-actin complex appears as full protein (CRM197, 58 kDa) and as subunits of CRM197; fragment B (37 kDa), fragment A (24 kDa) besides actin taking place in 43 kDa mass (Fig. 2B; lane 2). Western blot analysis carried out with anti-actin (lane 3) and anti-FA (lane 4) which showed both full protein CRM197 and its subunit, fragment A.

Docking benchmark studies and molecular dynamics simulation for CRM197-actin complex

Calculation of binding energies of CRM197 to actin, ClusPro 2.0, an automated protein docking server with molecular modeling program was used. Docked conformations were generated using DOT, the docking program based on FFT correlation approach. Default values of 1 Å gridstep and 4 Å surface layers were used. Docked complexes were se-

lected and ranked based on a hierarchical clustering method (Comeau et al. 2004). The structure of GRM197-actin complex was modelled in ClusPro server. In order to score the docking orientations electrostatic filter, residue pair potentials and biochemical data were included in addition to surface complementarity.

Data from our studies provide information for atomistic insight of CRM197–actin interaction. We have identified three hotspots and determined amino acids Lys42, Cys218, Cys233 of CRM197 forming contacts with Gly197, Arg62, Ser60, respectively. Molecular dynamics (MD) simulation of CRM197-actin complex was performed using the CHARMM force field (Brooks et al. 1983).

Both complexes of CRM197 and actin were subjected to all atom MD simulations to verify the stability of the complex during a long MD run of 13 ns by using 31.316 water molecules and also to calculate the ensemble average of binding free energy between CRM197 and actin from the MD trajectories. RMSD for all backbone atoms, electrostatic energy, van der Waals energy of CRM197-actin complex were studied in the form of MD trajectories. RMSD profiles always remained less than 0.5 nm for the entire simulation. The RMSD value for CRM197-actin complex increased from 0.042 to 0.27 nm at 3.2 ns, further constantly increased to attain 0.33 nm values at 10 ns and finally attained 0.5 nm around 13 ns depicting a constant RMSD profile during
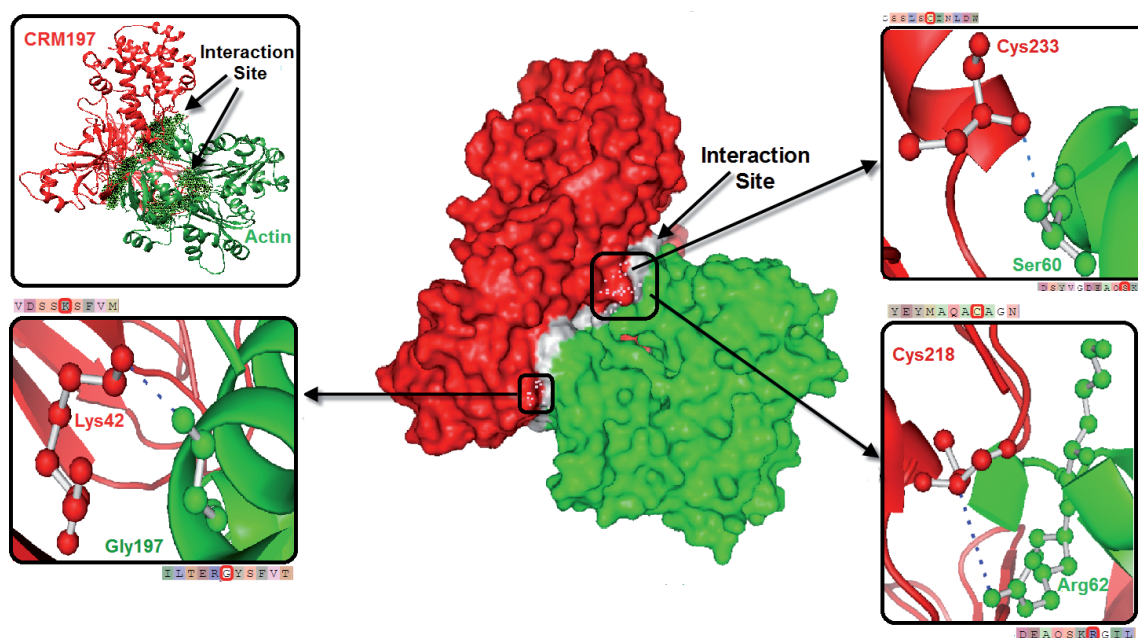

Figure 3. CRM197-G-actin interaction from molecular docking and MD simulation studies. CRM197-G-actin docked complex has been shown in cartoon structure. CRM197 and G-actin has been shown in red and green color, respectively. Interaction site of CRM197-G-actin complex showed in ribbon representation has been replaced upper left. Magnified view of three hot points is shown in the inset. The interacting amino acids are emphasized in sticks/spheres. Blue dashed lines indicate the bond between CRM197-G-actin complexes. Sequence alignment of both interacting structures is also indicated.

simulation. Theoretical model of amino acids contacts in CRM197-actin complex (within 2.1 Å–3.4 Å) are shown in Figure 3. According to docking benchmark studies and MD simulation for CRM197-actin complex three hot spots were found and free energies between these hot spots were determined as Ser60 and Cys233 (DG = –17.32 kJ/mol), Gly197 and Lys42 (DG = –11.26 kJ/mol), Arg62 and Cys218 (DG = –8.32 kJ/mol).

Discussion

In this study, we have shown actin cytoskeleton rearrangement in endothelial cells upon CRM197 treatment *in vitro*. To address the interaction between CRM197 and actin, both experimental and theoretical studies were carried out. Our findings indicate widespread distribution of CRM197 on actin filaments in cultured endothelial cells. Colocalization of CRM197 with actin filaments supports the finding of molecular interaction that is required for endocytosis of DTx. Moreover, CRM197 differs from DTx which has been shown to be localized in perinuclear area of HUVECs (Bektaş et al. 2011). Our results of gel filtration and Western blot analysis show that CRM197 can interact with G-actin. This outcome is supported by previously reported *in vitro* and *in vivo* binding effect of CRM197 to F-actin (Varol et al. 2012). It has been reported that interactions between actin cytoskeleton and elements of protein synthetic machinery mediate delivery of DTx (Varol et al. 2013). The catalytic domain (residues 1–193) of native toxin is translocated from endosomal compartment *via* T-domain (residues 200–387). Tyr204 of native toxin has been shown to interact with Gly48 of G-actin through studies of molecular dynamics simulations (Ünlü et al. 2013). Our docking benchmark studies and molecular dynamics simulations for CRM197-actin complex indicate three hot spots. These hot spots of amino acids are Lys42, Cys218, Cys233 of CRM197 forming contact with Gly197, Arg62, Ser60 of actin, respectively. Possible interaction between Lys42 of CRM197 with Gly197 of actin is compatible with binding experiments of FA-actin complex showing nearly 1 binding site is present on G- and F-actin for FA of native toxin (Bektaş et al. 2009). Amino acids residues 200–387 on CRM197, corresponding to T-domain of DTx, embody two cysteine residues to interact with actin which shows that actin cytoskeleton provides a structural framework also for endosomal traffic of CRM197.

It has been known for a long time that CRM197 has nuclease activity (Bruce et al. 1990) and actin possesses DNAse I-binding loop (Carlier et al. 2015). Our findings show that CRM197 share the same binding domain on actin with DNAase I. CRM197 may exert its nuclease activity by actin-based nuclear transport. Transport of p53, tumor suppressor protein, is an example of actin–based nuclear transport. It has been determined recently that monomeric is responsible for transport of p53 to perinuclear area (Saha et al. 2016).

Actin cytoskeleton is affected also indirectly by bacterial toxins trough Rho family proteins (Aktories et al. 2012). Several bacterial protein toxins like clostridial binary toxins target actin cytoskeleton for post-translational modifications. Glucosylation, adenylylation, ADP-ribosylation and deamidation are bacterial modifications of Rho GTPases which inactivate enzymatic activity, and consequently, actin cytoskeleton is disorganized. It has been shown that bacterial modifications of Rho GTPases are sensed by Pyrin through downstream modifications in the actin cytoskeleton pathway (Xu et al. 2014). In addition to Rho GTPases-controlled signaling pathways cross-linked actin oligomers are proposed to activate new toxicity pathways. Low abundant toxin effect has been recently shown to be amplified by upstream actin regulatory proteins mediated by cross-linked actin oligomers which are formed due to actin cross-linking domain of several toxins such as cholera, pertussis, and anthrax toxins (Heisler et al 2015). DTx catalyses the transfer of ADP-ribosyl group of NAD to eEF2 in addition both DTx and CRM197 depolymerize F-actin filaments (Varol et al. 2012). In the case of DTx protein synthesis inhibition is accompanied by actin cytoskeleton derangement.

The non-toxic mutant form of diphtheria toxin, CRM197 has been shown to damage F-actin but it is unknown whether it exerts any effect on Rho family protein or actin regulatory proteins.

In our study, CRM197 binding to G-actin, colocalization of CRM197 with actin filaments and the loss of cell-cell contact show that actin comes into sight as target molecule for CRM197. In conclusion, CRM197 damages actin cytoskeleton, therefore, would enhance cell motility, and subsequently, limit cell-to-cell communication. We suggest that changes in actin cytoskeleton of endothelial cells under the treatment of CRM197 may underlie the previously reported effect of CRM197 for cargo transfer across blood-brain barrier to central nervous system.

References

Aktories K., Schwan C., Papatheodorou P., Lang A. E. (2012): Bidirectional attack on the actin cytoskeleton. Bacterial protein toxins causing polymerization or depolymerization of actin. Toxicon **60,** 572–581
https://doi.org/10.1016/j.toxicon.2012.04.338

Bektaş M., Varol B., Nurten R., Bermek E. (2009): Interaction of diphtheria toxin (fragment A) with actin. Cell Biochem. Funct. **27,** 430–439
https://doi.org/10.1002/cbf.1590

Bektaş M., Hacıosmanoğlu E., Özerman B., Varol B., Nurten R., Bermek E. (2011): On diphtheria toxin fragment A release into the cytosol–cytochalasin D effect and involvement of actin filaments and eukaryotic elongation factor 2. Int. J. Biochem. Cell Biol. **43,** 1365–1372
https://doi.org/10.1016/j.biocel.2011.05.017

Bröker M., Costantino P., DeTora L., McIntosh E. D., Rappuoli R. (2011): Biochemical and biological characteristics of cross–reacting material 197 CRM197, a non–toxic mutant of diphtheria toxin: use as a conjugation protein in vaccines and other potential clinical applications. Biologicals **39,** 195–204
https://doi.org/10.1016/j.biologicals.2011.05.004

Brooks B. R., Bruccoleri R. E., Olafson B. D., States D. J., Swaminathan S., Karplus M. (1983): Charm: a program for macromolecular energy minimization, and dynamics calculations. J. Comput. Chem. **4,** 187–217
https://doi.org/10.1002/jcc.540040211

Bruce C., Baldwin R. L., Lessnick S. L., Wisnieski B. J. (1990): Diphtheria toxin and its ADP-ribosyltransferase-defective homologue CRM197 possess deoxyribonuclease activity. Proc. Natl. Acad. Sci. U.S.A. **87,** 2995–2998
https://doi.org/10.1073/pnas.87.8.2995

Carlier M. F., Pernier J., Montaville P., Shekhar S., Kühn S., Cytoskeleton Dynamics and Motility group (2015): Control of polarized assembly of actin filaments in cell motility. Cell Mol. Life Sci. **72,** 3051–3067
https://doi.org/10.1007/s00018-015-1914-2

Chen Y., Liu L. (2012): Modern methods for delivery of drugs across the blood–brain barrier Adv. Drug Deliver Rev. **64,** 640–665
https://doi.org/10.1016/j.addr.2011.11.010

Comeau S. R., Gatchell D. W., Vajda S., Camacho C. J. (2004): ClusPro: a fully automated algorithm for protein-protein docking. Nucleic Acids Res. **32,** W96–99
https://doi.org/10.1093/nar/gkh354

Giannini G., Rappuoli R., Ratti G. (1984): The amino–acid sequence of two non–toxic mutants of diphtheria toxin: CRM45 and CRM197. Nucleic Acids Res. **12,** 4063–4069
https://doi.org/10.1093/nar/12.10.4063

Heisle D. B., Kudryashova E., Grinevich D. O., Suarez C., Winkelman J. D., Birukov K. G., Kotha S. R., Parinandi N. L., Vavylonis D., Kovar D. R., Kudryashov D. S. (2015): ACTIN-DIRECTED TOXIN. ACD toxin-produced actin oligomers poison formin-controlled actin polymerization. Science **349,** 535–539
https://doi.org/10.1126/science.aab4090

Kageyama T., Ohishi M., Miyamoto S., Mizushima H., Iwamoto R., Mekada E. (2007): Diphtheria toxin mutant CRM197 possesses weak EF2–ADP–ribosyl activity that potentiates its anti–tumorigenic activity. J. Biochem. **142,** 95–104
https://doi.org/10.1093/jb/mvm116

Kozakov D., Brenke R., Comeau S. R., Vajda S. (2006): PIPER: an FFT-based protein docking program with pairwise potentials. Proteins **65,** 392–406
https://doi.org/10.1002/prot.21117

Laemmli U. K. (1970): Cleavage of structural proteins during the assembly of the head of bacteriophage T4. Nature **227,** 680–685
https://doi.org/10.1038/227680a0

Malito E., Bursulaya B., Chen C., Lo Surdo P., Picchianti M., Balducci E., Biancucci M., Brock A., Berti F., Bottomley M. J., Nissum M., Costantino P., Rappuoli R., Spraggon G. (2012): Structural basis for lack of toxicity of the diphtheria toxin mutant CRM197. Proc. Natl. Acad. Sci. U.S.A. **3,** 5229–5234
https://doi.org/10.1073/pnas.1201964109

Pierce B. G., Hourai Y., Weng Z. (2011): Accelerating protein docking in ZDOCK using an advanced 3D convolution library. PLoS One **6,** e24657
https://doi.org/10.1371/journal.pone.0024657

Qiao J., Ghani K., Caruso M. (2008): Diphtheria toxin mutant CRM197 is an inhibitor of protein synthesis that induces cellular toxicity. Toxicon. **51,** 473–477
https://doi.org/10.1016/j.toxicon.2007.09.010

Saha T., Guha D., Manna A., Panda A. K., Bhat J., Chatterjee S., Sa G. (2016): G-actin guides p53 nuclear transport: potential contribution of monomeric actin in altered localization of mutant p53. Sci. Rep. **6,** 32626
https://doi.org/10.1038/srep32626

Shinefield H. R. (2010): Overview of the development and current use of CRM197 conjugate vaccines for pediatric use. Vaccine **28,** 4335–4339
https://doi.org/10.1016/j.vaccine.2010.04.072

Tang X., Deng S., Li M., Lu M. (2016): Cross-reacting material 197 reverses the resistance to paclitaxel in paclitaxel-resistant human ovarian cancer. Tumor Biol. **37,** 5521–5528
https://doi.org/10.1007/s13277-015-4412-0

Ünlü A., Bektaş M., Şener S., Nurten R. (2013): The interaction between actin and FA fragment of diphtheria toxin. Mol. Biol. Rep. **40,** 3135–3145
https://doi.org/10.1007/s11033-012-2387-0

Ünlü A. (2014): Computational prediction of actin-actin interaction. Mol. Biol. Rep. **41,** 355–364
https://doi.org/10.1007/s11033-013-2869-8

Varol B., Bektaş M., Nurten R., Bermek E. (2012): The cytotoxic effect of diphtheria toxin on the actin cytoskeleton. Cell Mol. Biol. Lett. **17,** 49–61
https://doi.org/10.2478/s11658-011-0036-6

Varol B., Özerman Edis B., Bektaş M. (2013): Toxin structure, delivery and action. In: Corynebacterium Diphtheriae and Related Toxigenic Species. (Ed. A. Burkovski), pp. 83–94, Springer, Netherlands

Vinante F., Rigo A. (2013): Heparin-binding epidermal growth factor-like growth factor/Diphtheria toxin receptor in normal and neoplastic hematopoiesis. Toxins **5,** 1180–1201
https://doi.org/10.3390/toxins5061180

Xu H., Yang J., Gao W., Li L., Li P., Zhang L., Gong Y. N., Peng X., Xi J. J., Chen S., Wang F., Shao F. (2014): Innate immune sensing of bacterial modifications of Rho GTPases by the Pyrin inflammasome. Nature **513,** 237–241
https://doi.org/10.1038/nature13449